

Review

# Aptamer-Conjugated Quantum Dot Optical Biosensors: Strategies and Applications

Dongmin Kim <sup>1</sup> and Seungmin Yoo <sup>2,\*</sup> <sup>1</sup> Center for Applied Life Science, Hanbat National University, Daejeon 34158, Korea; dmk.iqbio@gmail.com<sup>2</sup> School of Integrative Engineering, Chung-Ang University, Seoul 06974, Korea

\* Correspondence: yooseun1@cau.ac.kr

**Abstract:** Quantum dots (QDs) represent the promising new generation of luminophores owing to their size-, composition-, and surface-dependent tunable photoluminescence (PL) and photochemical stability. The development of various QD composites with high PL and good biocompatibility has facilitated the use of aptamer-functionalized QD biosensors for highly sensitive and specific detection of molecules in clinical and environmental settings. In addition to describing the recent advances in aptamer-based QD biosensor technology for the detection of diverse chemicals and biomolecules, this review provides recent examples of sensing strategies based on optical signal enhancement and quenching of QDs. It also discusses potential strategies for the development of biosensors to widen their practical applications across various scientific and technological fields.

**Keywords:** quantum dot; aptamer; detection; biomolecule; photoluminescence; biosensor

**Citation:** Kim, D.; Yoo, S.Aptamer-Conjugated Quantum Dot Optical Biosensors: Strategies and Applications. *Chemosensors* **2021**, *9*, 318. <https://doi.org/10.3390/chemosensors9110318>

Academic Editor: Gabriella Leo

Received: 26 October 2021

Accepted: 10 November 2021

Published: 12 November 2021

**Publisher's Note:** MDPI stays neutral with regard to jurisdictional claims in published maps and institutional affiliations.



**Copyright:** © 2021 by the authors. Licensee MDPI, Basel, Switzerland. This article is an open access article distributed under the terms and conditions of the Creative Commons Attribution (CC BY) license (<https://creativecommons.org/licenses/by/4.0/>).

## 1. Introduction

Numerous pathogens and toxins exist in clinics, food industries, the environment, and military settings. These dangerous pollutants, including pathogenic bacteria, viruses, and heavy metals, can damage organ function and even cause failure, thereby seriously threatening people's health. Accurate and rapid detection of these dangerous molecules is of great importance in medical and diagnostic fields, allowing for early diagnosis and proper treatment/removal of medical and environmental conditions. To effectively detect and monitor the molecules in a practical setting, the sensing systems to be developed need to fulfil diverse requirements, such as sensitivity, specificity, multiple detection, real-time detection, and low cost.

Biosensors integrated with various nanomaterials offer several advantages, including low limit of detection (LoD), real-time analysis, and multiplex detection [1–3]. As novel nanomaterials are being developed rapidly, various types of sensing nanoplatfroms, physiochemical methods, bioconjugation strategies, and binding ligands are also being employed, leading to the creation of new strategies to enhance detection performance [4].

Nanomaterials that exhibit distinct optical, electrical, electrochemical, and magnetic characteristics have been applied for the development of biosensors that can detect and monitor dangerous pollutants [3,5–11]. These biosensors have been built using various nanomaterials, including nanoparticles (NPs), nanorods, nanowires, and quantum dots (QDs), as well as carbon-based nanomaterials, such as carbon dots (CDs), carbon nanotubes (CNTs), and graphene oxide (GOx) [5–12]. Of these, QDs possess unique spectral characteristics and act as special inorganic luminophores; therefore, they have come into focus to be used in the development of highly sensitive biosensors [12,13]. In addition to facilitating practical and sensitive detection, they also enable the monitoring of various molecules in environmental and clinical samples, including living cells [12–16]. This is a result of their several advantages over other fluorescence dyes, including their small size, wide excitation spectrum, narrow emission spectrum, and chemical resistance [17–19]. Varying the size,

shape, and composition allows the creation of diverse QDs with unique photoluminescence (PL) at tunable wavelengths across the visible and near-infrared (NIR) spectra.

In order to achieve high specificity of biosensors, numerous efforts have been devoted to the discovery and modification of various ligands, including peptides, phages, oligonucleotides, proteins, antibodies, and aptamers [3]. Among these ligands, aptamers are short, single-stranded DNA (ssDNA), RNA (ssRNA), or XNA (xeno nucleic acid, which is a synthetic nucleic acid analogue) [20,21] molecules that can selectively bind to a wide variety of target molecules including small chemicals, peptides, proteins, and even whole cells [22–26]. Aptamers can be screened through an iterative in vitro process called systematic evolution of ligands by exponential enrichment (SELEX). In the SELEX process, a large oligonucleotide pool used as starting materials is exposed with target molecules and an aptamer with high affinity against target molecules is isolated by various screening strategies [22–26]. Such selected aptamers exhibit high affinity, specificity, high thermostability, acid-base resistance, low immunogenicity and toxicity, low cost, and easy synthesis and modification [27–30]. These excellent properties have enabled their increased use as bio-recognition ligands for practical applications in industrial, environmental, and clinical settings. Their widespread use has further facilitated the creation of novel strategies and enhanced technologies for aptamer discovery, even the establishment of several companies dedicated to the discovery and synthesis of aptamers [22].

Several reviews provide detailed information on the principles and characteristics of QD biosensors [13,14,17,31]. This article focuses on introducing molecule detection strategies and technologies based on the factors that affect the change in the optical signal emission of QDs, which can be largely divided into the following four categories: (1) the aptamer-analyte binding event, (2) the materials directly attach to the aptamer, (3) the materials indirectly linked with the aptamer, and (4) the DNA-modifying enzymes involved in signal amplification and quenching. Representative applications of aptamer-based QD biosensors, including those described in this paper along with others that have been developed and employed for the detection of a wide range of molecules, are also detailed in Table 1. Furthermore, this review describes an approach that can enable the development of QD biosensors to help achieve their eventual practical use.

## 2. Aptamer-Based QD Biosensors for Molecule Detection and Monitoring

### 2.1. QD as Sensing Material

QDs are tiny semiconducting particles or nanocrystals with diameters of 2–10 nm, comprising 10–50 atoms [13,14,32]. Their small size and ability to operate in a confined space lead to the quantum confinement effect, by which QDs have a distinct energy level. The decreased particle size increases the difference in energy between the top of the valence band and the bottom of the conduction band, the so-called band gap. A wide band gap implies that more energy is required to excite the QDs, which concurrently means that they release more energy when returning to the ground level. When light or electric energy contacts the QD, the QD enters its excitation state, wherein the electron moves from a hole in the valence band to the conduction band. Recombination of the electron and the hole results in the release of a photon. The photon adsorption increases at higher energies in the QD, which provides it a broad absorption spectrum (300–800 nm) and longer fluorescent lifetime [33]. Its broad wavelength absorption spectrum allows PL to be excited in multiple QDs with different colors by a single excitation source. Owing to its broad wavelength absorption spectrum, the QD can utilize distance-dependent energy transfer phenomena, such as fluorescence resonance energy transfer (FRET) and nano surface energy transfer (NSET), through the introduction of other NPs such as AuNP as acceptors [34–36]. The high quantum yield of QDs result in high brightness and photochemical stability, making them resistant to chemical and photo degradation [37]. The distinct advantages of high molar extinction coefficients over a broad excitation region enable the simultaneous detection of multiple targets from the blue to NIR spectral region and the detection of molecules in living cells and tissues [38]. Recently, the multi-shelling process, which

involves coating semiconductor materials (shell) onto a colloidal QD (core), has facilitated the creation of diverse core-shell QDs, achieving higher fluorescence quantum yield and better photostability. The optical properties of QDs depend on their size, shape, material, composition of the core-shell conjugates, the shell growth rate, the additives, and the multiple emission layers [39–43].

## 2.2. Strategy for the Change in the Optical Signal Emission of the QDs for Biosensing Application

QD biosensors can detect and monitor the presence of an analyte in the samples based on their transition from the switch-on state to the switch-off state or vice versa. Biosensors are also capable of quantification, which is based on measuring the change in a tunable signal intensity. Ensuring clearer on-and-off detection and quantification requires this system to have a high signal intensity or low background noise in the initial state (without analyte). In aptamer-based QD biosensors, several systems that can harness the change in the optical signal emission of the QDs. The first system is based on the aptamer-analyte binding event [44–46]. Aptamer-attached QD emits an optical signal in the signal-on state. Once an analyte is added, the aptamer-analyte binding event occurs, and the aptamer-analyte quenches the emission of the QD, entering the signal-off state. In this strategy, the aptamer-analyte binding event triggers the signal on-off change in the system; therefore, this system has a simple and fast process. The binding force of the aptamer has a large kinetic barrier; therefore, it can significantly affect the sensing accuracy of the system.

The second system is based on the materials directly attaching to the aptamer [34,35]. This strategy usually harnesses the distance-dependent energy transfer mechanism. Aptamers are generally designed to attach to both QDs as emitters and the materials as quenchers. QD-aptamer-material composites maintain stretching, in which the QD-material distance is far enough to emit a signal from the QD, in its signal-on state. When an analyte exists in the sample, the aptamer binds to the analyte. As aptamer-target binding is determined by its tertiary structure, the binding event leads a conformational change in the aptamer which shortens the distance between the QD and the material, quenching the signal emission in the signal-off state. The binding ability of the aptamer and the quenching efficiency of the material facilitate the dynamic control of the system's sensing performance.

The third system is based on the materials indirectly linking to the aptamer [47,48]. Aptamers bind to QDs; however, the materials are combined with other nucleic acid strands with sequences complementary to the aptamers. Therefore, the materials can be linked to the aptamers only once the aptamers hybridize with the complementary strands, forming QD-aptamer:complementary strand duplex-material composites. In this case, the presence of an analyte breaks the aptamer:complementary strand duplex into two single-stranded oligos because of the preferable interaction of the aptamer against the analyte. Dissociation of the material-attached strand causes changes in the optical signal of the QD. Compared to two systems mentioned above, this system requires a rather complicated process; however, it enables more dynamic control of the QD signal by varying the lengths and number of complementary strands.

The fourth system is based on DNA-modifying enzymes [49–51]. This strategy generally utilizes multifunctional DNA fragments containing aptamers. The components of the DNA depend on the DNA-modifying enzyme that is to be used. In this strategy, after the aptamer-analyte binding event occurs, the addition of DNA-modifying enzymes triggers the target recycling and signal amplification reactions, which enhance the sensitivity and specificity even if small amounts of analyte exist in the sample. The assay time required depends on the efficiency with which the enzymes catalyze the reaction on the substrate. This can also help determine whether the DNA and the enzymes should be added to the reaction mixture consecutively or simultaneously. Although one-tube enzymatic reactions are simple, they can have low signal-to-noise ratios. Subsequent exogenous component addition can provide high signal-to-noise ratios; however, this requires a more complicated, multi-step process with a long assay time that can prevent its practical applications.

### 3. Current Aptamer-Based QD Biosensors for Chemical and Biomolecule Detection

In this section, we highlight how specific aptamer-based QD biosensors change the signal intensity of QD to detect various molecules. The challenges and strategies to improve the performance of these biosensors and the related parameters (linear range, LoD, etc.) are also summarized in [Table 1](#).

**Table 1.** Examples of aptamer-based QD biosensors for detection of various molecules <sup>a</sup>.

Sensing Platform	QD Material	Aptamer Conjugation Method	Analyte	Sensing Type	Linear Range	LoD	Sample	Features	Reference
Vinyl modified QD	Mn/ZnS	Conjugation of SH-aptamer to molecular imprinted polymer-QD	Cytochrome c (Cyt c)	Fluorescence	0.20–2.00 µM	54 nM	Urine, serum	Use of double recognition based on aptamer and imprinted cavity	[44]; Figure 1A
Polyethyleneimine (PEI)-capped core-shell QD	Mn/ZnS	Electrostatic attraction to (+) charged PEI-QD and (–) charged aptamer	Cyt c	PL	0.166–9.96 µM	84 nM	Human serum	Quenching effect by electron transfer between QD and Cyt c	[45]
Core/shell	PEG-CdSe/ZnS	Biotin aptamer-SA QD conjugation	EGFRvIII	Fluorescence	ND	ND	Mice bearing U87-EGFRvIII brain tumors	Small enough (20 nm) aptamer-QD conjugates to cross BBB	[52]
MNP-QD	CdTe	Hybridization of oligo with complementary strand of aptamer attached to QD	<i>Salmonella typhimurium</i>	Fluorescence	10–10 <sup>10</sup> CFU/mL	1 CFU/mL	Milk, water	Formation of MNP-QD composition by binding aptamer and complementary strand	[46]; Figure 1B
Core/shell	CdSe/ZnS	Covalent linking between COOH-QD and NH <sub>2</sub> -aptamer	Tumour necrosis factor-alpha (TNF-a)	PL	0–22.3 nM	97.2 pM	Human serum-based sample	Use of FRET. Sensing platform: QD (donor)-Aptamer-AuNP (acceptor)	[34]
Core/shell	CdSe/ZnS	Biotin aptamer-streptavidin QD conjugation	<i>Campylobacter jejuni</i>	Fluorescence	ND	5 CFU/mL	Chicken rinsate	Sandwich assay with aptamer-conjugated MB and aptamer-attached QD	[53]
Core/shell	CdSe/ZnS	Biotin aptamer-avidin QD conjugation	<i>Escherichia coli</i> O157:H7, <i>Salmonella typhimurium</i>	Fluorescence	63–10 <sup>8</sup> CFU/mL for <i>S. typhimurium</i> ; 40–10 <sup>8</sup> CFU/mL for <i>E. coli</i>	25 CFU/mL for <i>S. typhimurium</i> ; 16 CFU/mL for <i>E. coli</i>	Milk, human serum, human urine	Use of aptamer-modified fluorescentmagnetic multifunctional nanoprobe consisting of (3-mercaptopropyl) trimethoxysilane, magnetic γ-Fe <sub>2</sub> O <sub>3</sub> , and fluorescent QDs	[54]
Single QD	CdTe	Covalent linking between COOH-QD and NH <sub>2</sub> -aptamer	<i>S. typhimurium</i> , <i>Staphylococcus aureus</i>	PL	10–10 <sup>6</sup> CFU/mL	16 CFU/mL for <i>S. aureus</i> ; 28 CFU/mL for <i>S. typhimurium</i>	None	complementary strand-conjugated MB-aptamer-attached QD. Use of MB for simple separation	[55]
Core/shell	CdSe/ZnS	Covalent linking between COOH-QD and NH <sub>2</sub> -aptamer	TNF-a	PL	ND	ND	Mouse pre-osteocyte cells (MC3T3 E1), Mouse monocyte/macrophage cells (RAW264.7)	Use of FRET. Sensing platform: CPP-QD (donor)-Aptamer-AuNP (acceptor). Intracellular biomolecule detection	[35]; Figure 2
Core/shell	CdSe/ZnS	Covalent linking between COOH-QD and NH <sub>2</sub> -aptamer	Ca <sup>2+</sup>	PL	ND	3.77 pM	Mouse pre-osteocyte cells (MC3T3 E1)	Use of FRET. Complex sensing platform: CPP-QD (donor)-Aptamer-AuNP (acceptor). Intracellular biomolecule detection	[36]

Table 1. Cont.

Sensing Platform	QD Material	Aptamer Conjugation Method	Analyte	Sensing Type	Linear Range	LoD	Sample	Features	Reference
Single QD on GCE	CdS	Conjugation of SH-aptamer to QD-GCE	Thrombin	ECL	500–5000 pg/mL in quenching method; 50–2000 pg/mL in amplification method; 5–500 pg/mL in ratiometric method	92 pg/mL in quenching method; 6.5 pg/mL in amplification method; 500 fg/mL in ratiometric method	Human serum	Use of FRET. Enhancement of ECL emission of QD by treatment of H <sub>2</sub> O <sub>2</sub>	[56]
Single QD-GOx composite on GCE	CdS	Duplex formation with NH <sub>2</sub> -labelled complementary strand, which can bind to COOH-QD-GOx composite	Chloramphenicol	ECL	100 nM–1 pM	0.5 pM	Milk	Use of GOx-CdS QD-GCE as substrate. Use of HRP as quencher. Sensing platform: GCE-(GOx-QD)-Aptamer-HRP	[47]; Figure 3A
Core/shell on GCE	CdTe/CdS	Electrostatic attraction to NH <sub>2</sub> -QD and (-) charged aptamer	Thrombin	NECL	100 aM–10 fM	31 aM	Interfering agent (BSA, IgG, HSA)-containing samples	Coating of chitosan on GCE-QD for uniform surface for aptamer immobilization. Use of NIR QDs	[48]; Figure 3B
DNA-QD/AuNP	DNA	Conjugation of SH-aptamer to DNA-QD/AuNP conjugate	<i>S. typhimurium</i>	Fluorescence	10–1.0 × 10 <sup>7</sup> CFU/mL	13.6 CFU/mL	Milk	Use of DNA-QD/AuNP for easy and simple aptamer conjugation	[57]
Single QD on GCE	CdS	Covalent linking between COOH-QD and NH <sub>2</sub> -aptamer	Cardiac troponin I	ECL	1 fg/mL–10 ng/mL	0.75 fg/mL	Human serum	Use of aptamer conjugated CdS QDs and AuNPs as ECL luminophores and plasmon sources, respectively. Sandwich assay with aptamer-conjugated QD and aptamer-attached AuNP.	[58]
Core/shell on ITO electrode and magentic	CdTe/CdS	Covalent linking between COOH-QD and NH <sub>2</sub> -aptamer	Hg <sup>2+</sup>	ECL	20 aM to 2 μM	2 aM	Carp fish, saltwater fish, tap water	Sensing platform: Fe <sub>3</sub> O <sub>4</sub> @SiO <sub>2</sub> /dendrimers/QDs. Use of AuNP as a quencher.	[59]
MoS <sub>2</sub> @Pd-Au on GCE	MoS <sub>2</sub>	Duplex formation with primer DNA crosslinked with chitosan-MoS <sub>2</sub> @Pd-Au	Lipopolysaccharide	ECL	0.1 fg/mL–50 ng/mL	0.07 fg/mL	None	Incorporation of target-cycling synchronized rolling circle amplification reaction	[49]; Figure 4A
MoS <sub>2</sub> @Au	MoS <sub>2</sub>	Conjugation of SH-aptamer to QD	Siglec-5	ECL	10–500 pM	8.9 pM	None	Use of ExoIII-assisted signal amplification of QD	[50]; Figure 4B
Single QD	CdSe	Covalent linking between COOH-QD and NH <sub>2</sub> -SSB, followed by binding with aptamer	Streptomycin	Fluorescence	0.1–100 ng/mL	0.03 ng/mL	Milk	Use of ExoI-assisted target recycling amplification	[51]; Figure 4C
Single QD	CdSe	Duplex formation, which can covalently bind to antibody-QD	Chloromycetin	Fluorescence	0.05–100 ng/mL	2 pg/mL	Milk	Reusable sensing platform	[60]

<sup>a</sup> Abbreviations: QD, quantum dot; LoD, limit of detection; CPP, cell penetrating peptide; CFU, colony forming unit; MNP, magnetic nanoparticle; AuNP, gold nanoparticle; MB, magnetic bead; PL, photoluminescence; ECL, electrochemiluminescence; FRET, fluorescence resonance energy transfer; GOx, graphene oxide; GCE, glassy carbon electrode; NECL, near-infrared electrochemiluminescence; EGFRvIII, epidermal growth factor receptor variant III; BSA, bovine serum albumin; IgG, immunoglobulin G; HSA, human serum albumin; NIR, near-infrared; NPL, near-infrared PL; BBB, blood-brain barrier; ITO, Indium tin oxide; Siglec-5, sialic acid-binding immunoglobulin (Ig)-like lectin 5; ExoIII, exonuclease III; SSB, single-stranded DNA-binding protein; ExoI, exonuclease I; ND, not determined.

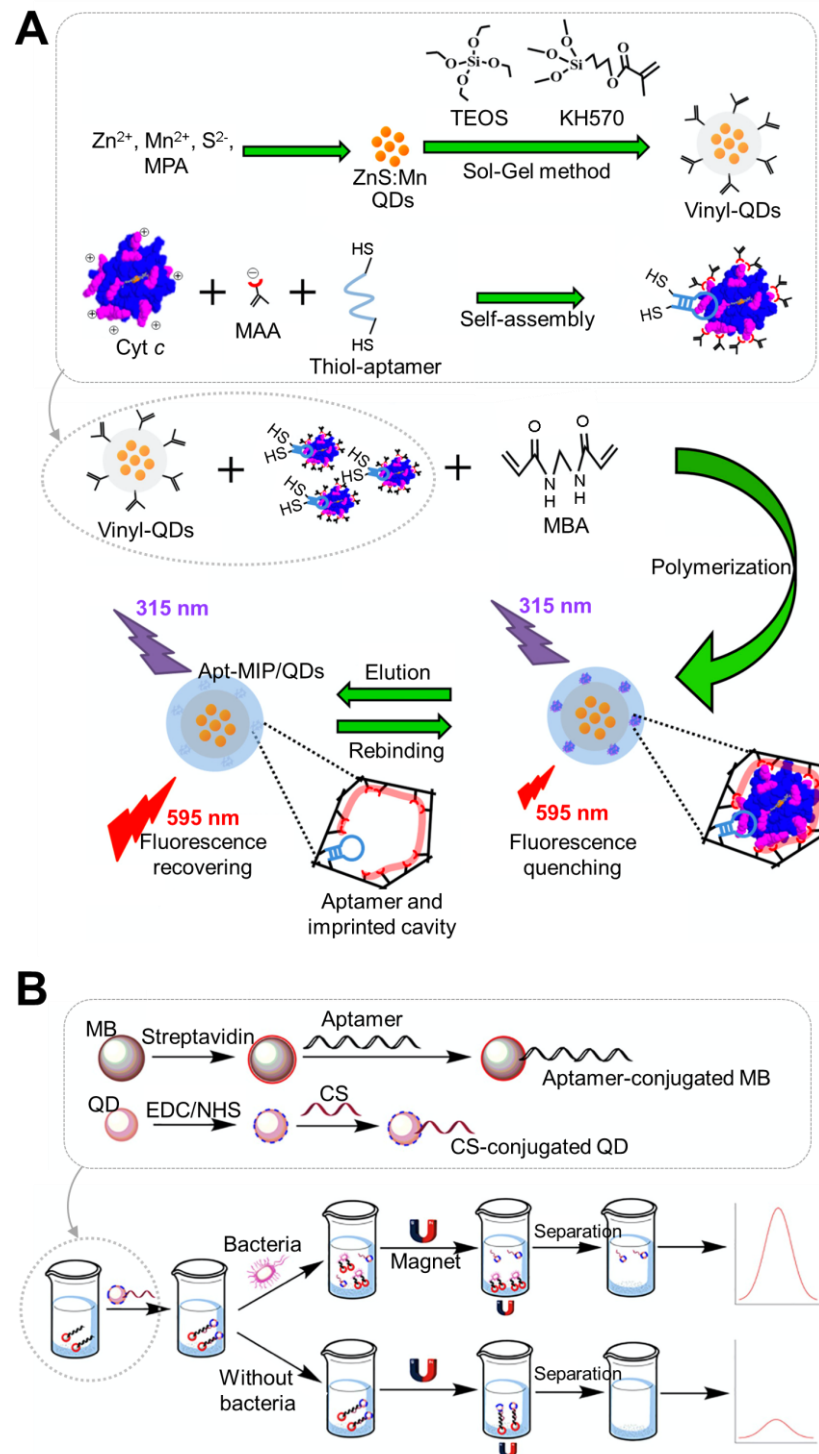


**Figure 1.** Quantum dot (QD) biosensing strategy based on change in optical signal of QD by aptamer-analyte binding: **(A)** Vinyl modified Mn/ZnS QD biosensor for detection of cytochrome c. Reproduced with permission from [44]; **(B)** magnetic nanoparticle-CdTe QD biosensor for detection of *Salmonella typhimurium*. Reproduced with permission from [46]. MPA, 3-Mercaptopropionic acid; TEOS, tetraethoxysilane; KH570,  $\gamma$ -methacryloxypropyl trimethoxy silane; MAA, methacrylic acid; MBA, N, N'-methylenebisacrylamine; EDC, 1-Ethyl-3-(3-dimethylaminopropyl) carbodiimide hydrochloride; NHS, N-hydroxysuccinimide; CS, complementary strand; MB, magnetic bead.

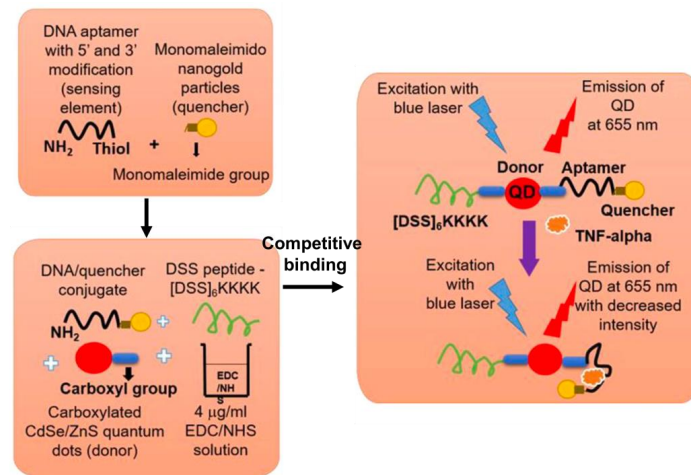


**Figure 2.** Quantum dot (QD) biosensing strategy based on change in optical signal of QD by materials directly attaching to the aptamer. CdSe/ZnS QD biosensor to the detection of intracellular tumour necrosis factor- $\alpha$  (TNF- $\alpha$ ). Reproduced with permission from [35]. EDC, 1-Ethyl-3-(3-dimethylaminopropyl) carbodiimide hydrochloride; NHS, *N*-hydroxysuccinimide.

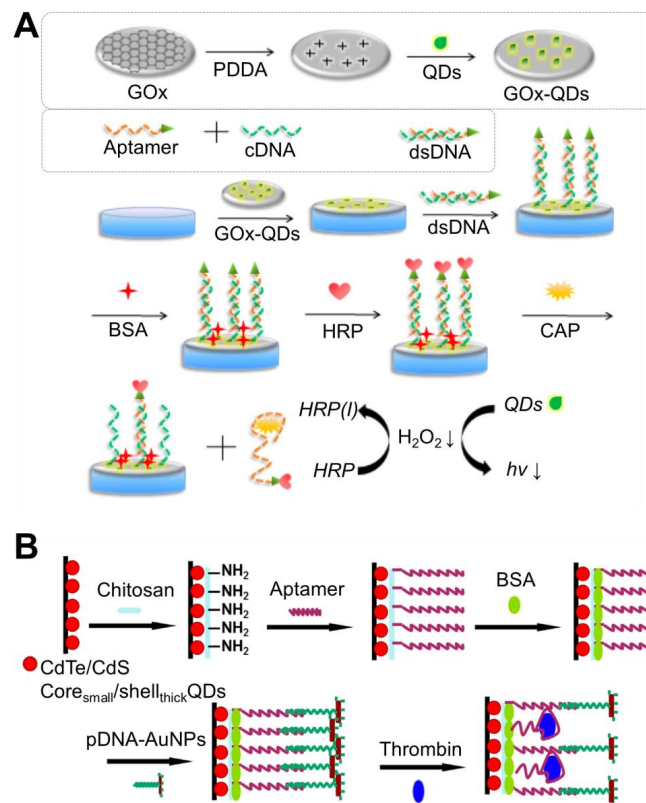


**Figure 3.** Quantum dot (QD) biosensing strategy based on change in optical signal of QD by materials indirectly linking with the aptamer (A) glassy carbon electrode (GCE)-deposited CdS QD-graphene oxide (GOx) composite biosensor to detect chloramphenicol. Reproduced with permission from [47]; (B) GCE-deposited CdTe/CdS QD biosensor to detect thrombin. Reproduced with permission from [48]. PDDA, Poly(diallyldimethylammonium chloride); cDNA, complementary DNA; dsDNA, double-stranded DNA; BSA, bovine serum albumin; HRP, horseradish peroxidase; CAP, chloramphenicol, pDNA-AuNP, probing DNA-modified gold nanoparticle.

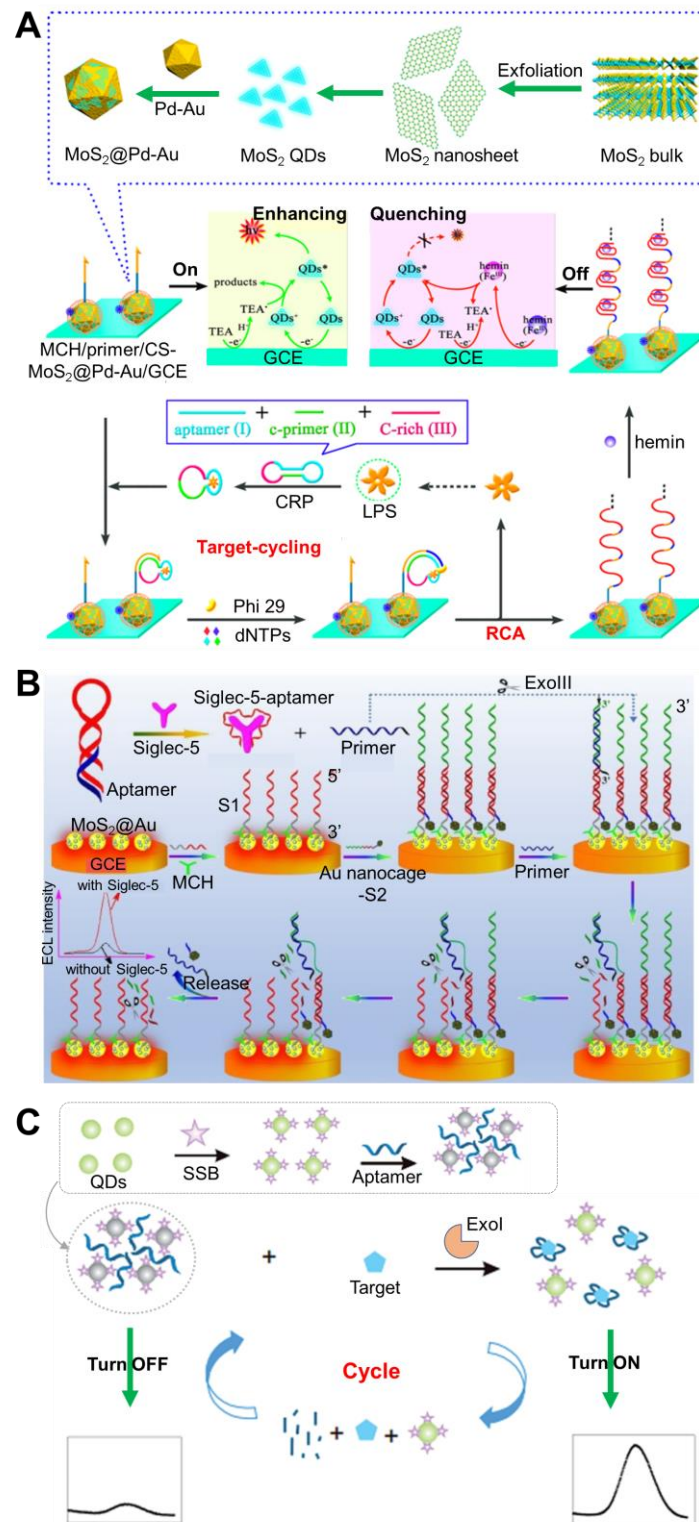


**Figure 4.** Quantum dot (QD) biosensing strategy based on change in signal emission of QD by DNA-modifying enzyme-assisted reaction. (A) Aptamer-driven target-cycling synchronized rolling circle reaction-coupled MoS<sub>2</sub>QD@Pd-Au composite biosensor for detection of lipopolysaccharide (LPS). Reproduced with permission from [49]; (B) exonuclease III (ExoIII)-based signal amplification reaction-coupled MoS<sub>2</sub>QD@Au composite biosensor to detect LPS. Reproduced with permission from [50]; (C) exonuclease I (ExoI)-aided target recycling reaction-coupled MoS<sub>2</sub>QD@Au composite biosensor to detect streptomycin. Reproduced with permission from [51]. GCE, glassy carbon electrode; TEA, trimethylamine; CRP, circular recognition probe; dNTP, deoxyribonucleoside triphosphate; RCA, rolling circle amplification; MCH, mercaptohexanol.

### 3.1. Biosensor Based on Change in Signal Emission of QD by Aptamer-Analyte Binding

The binding of aptamers with target molecules can directly change the signal emission of QDs. Aptamer-functionalized QDs can detect and monitor the presence of analytes by observing changes in the PL of the QDs. For example, an Mn-ZnS QD biosensor has been developed to detect cytochrome *c* (Cyt *c*) [44,45]. Mn doping can enhance the optical and electronic transport of QDs [61,62]. For the specific capture of Cyt *c*, the double recognition strategy was used; one recognition was achieved by using aptamers, and the other was achieved by using molecular imprinted polymers (MIPs) [44]; Figure 1A. MIPs are artificial custom-designed affinity materials. The polymerization of monomers upon exposure to template molecules forms a cavity in the polymer matrix, where the target molecules can bind, functioning as a lock-and-key mechanism [63]. In the fabrication of MIPs, aptamers have been used as target molecules [64], and these apt-MIP composites have been used to detect proteins and viruses [65,66]. This system, using thiolated DNA aptamers and methacrylic acid as the functional monomers, has been reported to form apt-MIP composites [44]. After cross-linking and polymerization, the imprinted cavity on the surface of the vinyl-QDs could specifically recognize the Cyt *c*, thereby quenching the fluorescence of the QDs. This system exhibited an LoD of 0.054  $\mu\text{M}$  with a linear range of 0.20–2.00  $\mu\text{M}$  (Table 1).

In order to detect Cyt *c* through easy and fast aptamer conjugation to QD, a QD was coated with polyethyleneimine (PEI) and then conjugated with an aptamer through the electrostatic interaction between the positively charged PEI and negatively charged DNA aptamer [45]. The added Cyt *c* made the aptamer form a ternary compound, and the electron transfer between the QD and Cyt *c* quenched the PL of the QD. This system could detect 84 nM of Cyt *c* with a detection range of 0.166–9.96  $\mu\text{M}$  (Table 1).

In another example, aptamers were attached to CdTe QDs through hybridization with complementary ssDNA, forming an aptamer:ssDNA duplex-QD composite [46]; Figure 1B. Exposing this composite to an analyte (*Salmonella typhimurium*) allowed the aptamer to preferentially bind to it, while dissociating from the composite. As the aptamer was functionalized with magnetic NPs, the released aptamer could be easily separated using a magnet, whereas the remaining QD could emit fluorescence. The system exhibited an LoD of 1 CFU/mL with a linear range of 10–10<sup>10</sup> CFU/mL (Table 1).

### 3.2. Biosensor Using Change in Signal Emission of QD by Materials Directly Attaching to the Aptamer

Materials that can cause a change in the optical properties of QDs can directly bind to an aptamer, where the aptamer can act as a linker bridging the QD and the material. As aptamers undergo changes in tertiary structure upon binding to analyte, the distance of QD and the material depends on an aptamer-analyte binding. Based on this phenomena, QD biosensors can harness the FRET effect to convert the switch-on state into the switch-off state or vice versa. FRET relies on the transfer of excitation energy of a donor fluorophore to an acceptor molecule through nonradiative dipole-dipole coupling. In FRET-based QD biosensor, QD and the material act as donor dye and acceptor molecules, respectively. The metallic QD-based system can be applied to another distance-dependent energy transfer, NSEF, which is a dipole-surface energy transfer process involving a metallic surface and a molecules dipole. The aptamer can modulate the distance between the donor and the acceptor; a conformational change in the aptamer shortens the distance, thereby quenching the QD emission. Based on this system, QDs can be used with various materials to detect or monitor dynamic binding events between aptamers and analytes.

A QD-NP composite can exhibit the FRET effect in the UV-visible range, where the QD acts as a donor and the NPs act as acceptors that can quench or cause a release of photons [34–36]. For example, intracellular tumor necrosis factor- $\alpha$  (TNF- $\alpha$ ) could be detected using the QD-AuNP sensing material [34]. The sensing platform comprised a QD, an AuNP, and an aptamer. The aptamer had two functional groups at each end; at one end, an amine group was attached, which bound to the carboxyl group-modified

CdSe/ZnS QD that functioned as the FRET donor. At the other end, a thiol group was labelled and bound to the monomaleimide AuNP that functioned as the FRET acceptor. In the absence of TNF- $\alpha$ , the QD was far enough away from the AuNP to emit its PL. This resulted from the large amount of energy available in the QD that could be emitted as photons because of little to no transfer of energy from the QD to the AuNP, as the quencher. Upon the exposure of TNF- $\alpha$ , the aptamer specifically bound to TNF- $\alpha$  and underwent a conformational change, which reduced the QD-AuNP distance, resulting in a decrease in PL intensity. The change in PL intensity depended on the concentration of the TNF- $\alpha$  in the sample. This system revealed a linear correlation in the range of 0–22.3 nM with a LoD of 97.2 pM (Table 1).

This system has been applied to detect intracellular biomolecules in living cells by introducing a cell-penetrating peptide [36,38]. The DSS (Asp-Ser-Ser) peptide is a well-known cell-penetrating peptide [67]; this repeated motif has been used to coat lignin NPs to improve drug delivery efficiency [38,68]. The use of the DSS peptide enhances cell entry efficiency without endosomal trapping. In the QD-AuNP sensing platform, the DSS peptide was attached to a carboxylated QD [35]; Figure 2. Upon the DSS peptide-assisted entry of the sensory molecules into the macrophage cells, they exhibited a high PL intensity from the QD. The PL intensity was significantly decreased when the cells were treated with bacterial lipopolysaccharide (LPS), which triggers TNF- $\alpha$  production by inducing infection and inflammation. Using the same system, intracellular Ca<sup>2+</sup> has been detected in living cells stimulated by thapsigargin, which induced increased intracellular calcium release [36]. This system could detect intracellular Ca<sup>2+</sup> up to 3.77 pM (Table 1).

### *3.3. Biosensor Using Change in Signal Emission of QD by Materials Indirectly Linking with the Aptamer*

Materials that influence the emission of photons from QDs can also indirectly bind to aptamers. Materials are generally attached to oligos with sequences complementary to the aptamers, which eventually form a duplex with aptamer. This system is designed to ensure that the duplex only partially forms base pairs while retaining ssDNA in some regions; therefore, adding target molecules can result in the preferential binding of aptamers to targets rather than to complementary strands, resulting in the dissociation of the duplex and the release of materials. Compared to the strategy in which the aptamer is directly attached, this strategy can exhibit dynamic changes in QD emission by changing the length of the duplex, and introducing another signal amplification/quenching reaction or fluorescent dye/luminophore.

For example, a ratiometric assay has been developed to detect thrombin by employing a QD-NP composite with luminol [56]. These ratiometric assays are based on the change in electrochemiluminescence (ECL) signals from two different luminophores depending on the concentration of the analytes [69–72]. In this method, two different thrombin-specific aptamers were used: aptamer I was modified with thiol at the 5' end to conjugate with the CdS QD and biotin at the 3' end to interact with the streptavidin-coated AuNPs, and aptamer II was functionalized with biotin at the 5' end to bind with the streptavidin-coated luminol-AuNP composites [56]. First, the CdS QDs were deposited onto the surface of the glassy carbon electrode (GCE), and aptamer I was sequentially attached to the QDs. When thrombin was present in the sample, aptamer I underwent a conformational change that reduced the distance between the QD and the AuNP, resulting in quenching of the CdS by the AuNPs. The presence of thrombin could be checked by observing the increased ECL intensity of luminol after introduction of the aptamer II-luminol-AuNP composites. The proximity of AuNP to luminol enhanced its ECL emission by increasing the electron transfer rate. In addition, to observe the obvious change in ECL intensity from the QD, it was pre-treated with H<sub>2</sub>O<sub>2</sub> which oxidizes the CdS QD, leading to the formation of excess Cd<sup>2+</sup> ions (sulphur vacancies) on the surface of the QD. This has been shown to stabilize the electrogenerated radicals, resulting in enhanced ECL intensity [73]. Treatment with citric acid has also been reported to enhance the stability of the QD, facilitating the formation of more excited states of QD. The system could detect 500 fg/mL of thrombin [56]; Table 1.

As a QD quencher, horseradish peroxidase (HRP) has been used to detect chloramphenicol [47]; Figure 3A. In order to immobilize CdS QD on the GCE, GOx was positively charged by treatment with polydiallyldimethylammonium chloride (PDDA) [74], which functioned as a linker. GOx could bind with CdS QD through electrostatic interactions and then the GOx-QD composite could be adsorbed onto the GCE. The amine-attached chloramphenicol-specific aptamer formed a duplex with its complementary strand, which is modified with biotin, resulting in two functional groups. The first functional group, amine, enabled the binding of aptamer with the carboxyl group of the QD. The second group, biotin, bound with streptavidin-coated HRP. When the sensing platform was exposed to a solution containing  $H_2O_2$ , the  $H_2O_2$  reacted with the electron-injected QD to generate excited QDs, leading to strong ECL intensity because of signal amplification. In the presence of HRP, the  $H_2O_2$  was consumed and the ECL intensity decreased, indicating that HRP could quench excited states of QD [74]. The presence of chloramphenicol led to a conformational change in the aptamer, causing it to be released from the duplex; eventually, the HRP attached to the aptamer was also removed in the washing step, resulting in an increase in the ECL intensity.

In addition to the application of QDs as visible-range ECL biosensors, there have been efforts to broaden the application of QD biosensors that are capable of detection in the NIR range. NIR emitters have several advantages including minimal autofluorescence, light absorption, and scattering from the biological environment, which have facilitated the development of NIR QDs [75]. In order to detect biomolecules in the NIR range, an aptamer-based QD biosensor has been incorporated with gold nanorods (AuNRs), which exhibit distinct shape-dependent surface plasmon resonance [48]; Figure 3B. A nanorod can absorb light in the NIR region; therefore, it can function as a FRET acceptor [76]. When molecules are detected in the NIR range, the background signal is extremely low, enabling interference-free detection, especially in complex biological samples [77]. For example, an NIR ECL (NECL)-emitting QD biosensor has been applied to detect thrombin [48]. For NECL detection, CdTe/CdS QDs have been coated on the surface of a GCE to obtain strong and stable NECL emission. The resulting QDs-GCE was pre-treated with a chitosan solution to obtain a uniform substrate surface, which enables uniform DNA immobilization, resulting in good reproducibility. Aptamers have been immobilized on QDs-GCE substrate through electrostatic attraction to  $NH_2$ -QD and subsequent formation of a partial duplex with another DNA (pDNA) with a sequence complementary to the aptamer. The formation of a partial duplex resulted in a decrease in NECL emission because the end of the pDNA was linked to the AuNRs. When thrombin was present in the sample, it could specifically bind to the aptamer, which underwent conformational change and detached pDNA-AuNR from the aptamer, resulting in an increase in NECL intensity from the QD. In order to enhance the ECL energy transfer efficiency, which directly affects LoD, two different factors were optimized: one factor was the spectrum overlap between the donor and acceptor, which was optimized by employing pDNA-AuNRs with longitudinal surface plasmon resonance (SPR) bands at different wavelengths. The other was the distance between the QD and AuNR [78,79], which was optimized by changing the length of aptamer-pDNA. Therefore, using the low background noise of NIR-emitting QDs and a specific aptamer in optimal condition with enhanced ECL efficiency yielded a high LoD of 31 aM for thrombin (Table 1).

### *3.4. Biosensor Using Change in Signal Emission of QD by DNA-Modifying Enzyme-Assisted Reaction*

The optical signals of QDs can be altered by incorporating an enzymatic catalytic reaction. The distinct catalytic activities and enzymatic activities of DNA-modifying enzymes, including DNA polymerases, nicking endonucleases, and exonucleases, can be used to enhance signal amplification and quenching because of their specific recognition capabilities and characteristic functional mechanisms [80]. The QD biosensor that uses aptamer-driven target cycling synchronized rolling circle amplification (RCA) reaction is one example. Using this sensor, LPS could be detected up to 70 ag/mL [49]; Figure 4A;

Table 1. This system used MoS<sub>2</sub> QDs that were encapsulated with a Pd-Au hexoctahedron composite and coated with chitosan. After activating the chitosan film for crosslinking with amine-functionalized primer DNA, dumbbell-shaped DNA was added. This DNA comprised multifunctional parts: a c-primer region with a sequence complementary to the primer, an aptamer region to specifically bind LPS, and a C-rich domain to form the hemin/G-quadruplex. Upon adding dumbbell-shaped DNA, this DNA could bind to the primer DNA at the c-primer region. When the analyte was present in the sample, the analyte bound to the aptamer region of the dumbbell-shaped DNA. After phi 29 polymerase and dNTPs were added, the dumbbell-shaped DNA acted as a template for the rolling circle amplification, and the primer strand on the MoS<sub>2</sub>/Pd-Au composite QD was lengthened. During RCA reaction, the analyte was released from the dumbbell-shaped DNA and bound to another dumbbell-shaped DNA, which is called the target-recycling reaction. As the generated RCA product, the lengthened primer on the composite QD contained numerous C-rich domains, which embed hemin, resulting in the quenching of the ECL emission from the QDs.

Another example is the incorporation of the exonuclease III-assisted signal amplification reaction. This sensor could achieve an LoD of LPS as low as 8.9 pM [50]; Figure 4B; Table 1. The QD used in this method was MoS<sub>2</sub>, which is an ECL emitter with low toxicity and good biocompatibility; however, it has limited intrinsic conductivity and functional groups on the surface [50,81,82]. These limitations can be overcome by forming a composite with AuNP, which provides a large area to attach and facilitates the immobilization of various chemicals, especially thiolated aptamers, through the formation of an Au-S covalent bond [83]. The MoS<sub>2</sub>@Au composite QD was deposited onto the GCE and conjugated with an ssDNA: Au nanocage-attached DNA (Au nanocage-S2) duplex; therefore, this activated the off state because of the quenching of the QD's ECL emission by the Au nanocage [50]. When LPS was present, the aptamer:primer duplex was dissociated by preferentially binding the aptamer and the LPS, releasing the primer and further binding another Au nanocage-S2 that was already hybridized with S1 on MoS<sub>2</sub>@Au/GCE. Exposure of exonuclease III led to the specific cleavage of the 3' terminus of the dsDNA and caused the digestion of Au nanocage-S2, which was in the off state. Concurrently, the primer was released from the duplex, enabling the combination of another S2 at a different locus on MoS<sub>2</sub>@Au/GCE to trigger the next cycle. The repeated cycle enabled primer recycling and signal amplification. The use of the Au nanocage instead of AuNP made the transition of the signal on-off state clearer because the Au nanocage exhibited enhanced quenching efficiency because of higher overlap with the ECL spectra of this QD composite.

In another study, exonuclease I has been employed in a biosensor to detect streptomycin [51]; Figure 4C. The signal-off state of the biosensor was achieved by the interaction between an ssDNA-binding protein (SSB)-attached QD and the aptamer. SSB could specifically bind to the ssDNA aptamer and act as a linker bridging the QDs, resulting in QD aggregation and quenching the fluorescence emission of the QD, which was in the signal-on state. Upon the addition of streptomycin and exonuclease I, the aptamer could preferentially bind with streptomycin, and the aptamer-free SSB-QD dispersed into solution, entering the signal-on state. Exonuclease I digested the aptamer coupled with streptomycin, and the liberated streptomycin could combine with another aptamer-SSB-QD aggregate. This system achieved an LoD of 30 pg/mL with a linear range of 0.1–100 ng/mL (Table 1).

#### 4. Conclusions and Future Perspectives

QDs have been widely applied to detect and monitor molecules *in vitro* and *in vivo* owing to their excellent optical properties, such as their small size, photostability, broad excitation spectra, and narrow emission spectra. Their broadened application has facilitated the development of QDs with novel compositions and structures. By selecting the particle size, shape, material, and composition, the PL emission band can be easily adjusted from UV to IR [39–41]. The optimization of the shell growth rate, additives, and multiple emitting layers can enhance the PL quantum yield and photostability, which allows sensitive

detection [42,43]. With these advances in QDs, the development of diverse nanostructure architectures, surface modifications [17], and aptamer-screening strategies [22] will play an increasingly critical role in the advancement of aptamer-based QD sensors to detect biomolecules in clinical and environmental settings.

Diverse in vitro biosensors were created with the development of various QDs triggered by the superior photophysical properties of QDs, and the tremendous progress. However, in developing in vivo biosensor, the toxicity and the biocompatibility of QDs are still major concerns for the detection of intracellular molecules in living cells or tissues. Most QDs are made using toxic materials, such as Cd, In, Te, and As, that can cause damage in multiple organ systems including the digestive, immune, nervous, and cardiovascular systems [82]. Many efforts have been devoted to overcoming these limitations (Table 2).

**Table 2.** Strategies for overcoming toxicity of QDs.

Purpose	Strategy	Feature	Reference(s)
Reduction of toxicity	Deposition of semiconductor shell layer on the core (production of core-shell composite)	Protection of the toxic component from degradation; Minimal surface defects of these QDs	[75]
	Attachment of hydrophilic bifunctional molecule (e.g., PEG)	High stability under biologically relevant conditions; Less affected by size of QD	[52,84,85]
	Functionalization of amphiphilic polymer (micelle-forming)	Robust, commercially available, and cheap polymeric precursors; Easy control over number of functional units introduced into polymeric coating	[86–88]
	Coating surface of QD with silica	Non-toxic, biocompatible, chemically inert, optically transparent, protect from leaching of toxic QD components	[89,90]
Use of eco-friendly synthetic method	Bacteria, fungi, virus-driven biosynthesis	Need for optimization of biosynthesis, recovery, and purification process	[91]
	• Use of bacteria	• CdS QD production from <i>Escherichia coli</i> , <i>Moorella thermoacetica</i> , <i>Acidithiobacillus</i> , <i>Pedobacter</i> sp., <i>Thermoanaerobacter</i> sp.	[92–95]
		• CdSAg QD production from <i>E. coli</i>	[96]
		• CdTe QD production from <i>E. coli</i>	[97]
		• ZnS QD production from <i>Thermoanaerobacter</i> sp.	[98,99]
	• Use of yeast	• CdS QD production from <i>Schizosaccharomyces pombe</i>	[100,101]
		• CdTe QD production from <i>Fusarium oxysporum</i> <i>Saccharomyces cerevisiae</i>	[102,103]
		• ZnS QD production from <i>Saccharomyces cerevisiae</i> and <i>Aspergillus</i> sp.	[104,105]
	• Use of virus	• Pt, Rh, Pd, Fe, Co, and Ni NPs production using T4 bacteriophage capsid	[106]
• ZnS and CdS QD production from M13 bacteriophage		[107]	

One way to reduce their toxicity is to change the surface of QDs. This surface change could be achieved through various fabrication strategies of core-shell conjugates because this can increase the size of the QDs and protect the toxic component from degrading, thereby minimizing the surface defects of these QDs and enhancing their luminescent quantum yield [75].

The QD surface can also be modified using three methods. One approach is ligand-based modification, where hydrophilic bifunctional molecules, such as PEG, are attached onto the surface of QDs [84,85]. This method is relatively simple and cost-effective, and it does not affect the change in particle size; however, it typically results in a lower PL quantum yield. For example, PEG-functionalized Cd-based QDs exhibited reduced toxicity

and biocompatibility while retaining a high PL quantum yield, where PEG formed a fence-like structure, resulting in prevention of  $\text{Cd}^{2+}$  accumulation on the QD surface [52,84]. CdSe/CdS QDs were also modified with PEG using a cascade treatment of 3-mercaptopropionic acid (MPA) thiol-terminated methoxy PEG (mPEG-HS), where the resultant QDs exhibited a decreased PL intensity, and upon adding glycine to the solution the original PL intensity was re-achieved [85]. Another approach is micelle formation, where an amphiphilic polymer surrounds the surface of the QD through hydrophobic interactions [86–88]. Unlike the surface change approach, encapsulation provides large QDs with a high quantum yield. The silanization method can decrease the toxicity of QDs by covering the surface of QDs in a silica shell [89,90]. The silica surface is non-toxic and relatively biocompatible and prevents the leaching of toxic QD components (e.g., Cd). Moreover, it can be easily functionalized for bioconjugation.

Concerns regarding the chemical production of QDs, which requires a high temperature, pressure, and hazardous solvents and ligands, remain the main obstacle to their broad biological application [91]. An alternative way to produce eco-friendly QDs is to use microorganisms or viruses [92–107].

Another advantage of bioproduction is that it provides biogenic QDs to functional groups such as -OH, -NH<sub>2</sub>, and C=O originating from various biomolecules without additional processes [108]. These functional groups also lower the toxicity and exhibit good biocompatibility.

Some QDs have been produced at large titers in industrial-scale production; for example, ZnS QDs and CdS QDs have been produced in quantities as high as 322 g (72% yield) and ~3 g/L in *Thermoanaerobacter* sp. in a batch fermentation reactor, respectively [98,99].

There are some challenges for shortening the time required for biosynthesis and to developing low-cost purification processes, including precipitation, extraction, centrifugation, and calcination. When the challenges described above are overcome, it is expected that biogenic QDs will be safely applied to more diverse and innovative applications across various fields without causing environmental pollution.

Although the current trend has shifted to the substitution of the common, toxic Cd- and Pb-based QDs for less toxic semiconductor nanocrystals, such as CuInS<sub>2</sub> and AgInS<sub>2</sub>, and the use of new material QDs such as silicon- and carbon-QDs [109–111], guidelines surrounding the safe handling of QDs are still needed during research, development, and large-scale manufacturing.

Taken together, these breakthroughs and innovations will undoubtedly lead to the emergence and discovery of new technologies and materials to facilitate disease diagnosis in the near future.

**Author Contributions:** Conceptualization, D.K. and S.Y.; writing, D.K. and S.Y.; supervision, S.Y.; funding acquisition, S.Y. All authors have read and agreed to the published version of the manuscript.

**Funding:** This work was supported by an NRF grant, funded by the Ministry of Science and ICT (grant number NRF-2019R1A2C1088504).

**Institutional Review Board Statement:** Not applicable.

**Informed Consent Statement:** Not applicable.

**Data Availability Statement:** No new data were created in this study. Data sharing is not applicable to this article.

**Conflicts of Interest:** The authors declare no conflict of interest.

## References

1. Mehrotra, P. Biosensors and their applications—A review. *J. Oral Biol. Craniofac. Res.* **2016**, *6*, 153–159. [[CrossRef](#)] [[PubMed](#)]
2. Alhadrami, H.A. Biosensors: Classifications, medical applications, and future prospective. *Biotechnol. Appl. Biochem.* **2018**, *65*, 497–508. [[CrossRef](#)] [[PubMed](#)]
3. Yoo, S.M.; Lee, S.Y. Optical Biosensors for the Detection of Pathogenic Microorganisms. *Trends Biotechnol.* **2016**, *34*, 7–25. [[CrossRef](#)] [[PubMed](#)]

4. Khalid, K.; Tan, X.; Zaid, H.F.M.; Tao, Y.; Chew, C.L.; Chu, D.-T.; Lam, M.K.; Ho, Y.-C.; Lim, J.W.; Wei, L.C. Advanced in developmental organic and inorganic nanomaterial: A review. *Bioengineered* **2020**, *11*, 328–355. [[CrossRef](#)]
5. Hubbe, H.; Mendes, E.; Boukany, P.E. Polymeric Nanowires for Diagnostic Applications. *Micromachines* **2019**, *10*, 225. [[CrossRef](#)]
6. Rahong, S.; Yasui, T.; Kaji, N.; Baba, Y. Recent developments in nanowires for bio-applications from molecular to cellular levels. *Lab Chip* **2016**, *16*, 1126–1138. [[CrossRef](#)]
7. Syedmoradi, L.; Ahmadi, A.; Norton, M.L.; Omidfar, K. A review on nanomaterial-based field effect transistor technology for biomarker detection. *Microchim. Acta* **2019**, *186*, 739. [[CrossRef](#)]
8. Saliev, T. The Advances in Biomedical Applications of Carbon Nanotubes. *C* **2019**, *5*, 29. [[CrossRef](#)]
9. Ansari, L.; Hallaj, S.; Hallaj, T.; Amjadi, M. Doped-carbon dots: Recent advances in their biosensing, bioimaging and therapy applications. *Colloids Surf. B Biointerfaces* **2021**, *203*, 111743. [[CrossRef](#)]
10. Ji, C.; Zhou, Y.; Leblanc, R.M.; Peng, Z. Recent Developments of Carbon Dots in Biosensing: A Review. *ACS Sens.* **2020**, *5*, 2724–2741. [[CrossRef](#)]
11. Yu, S.; Chen, T.; Zhang, Q.; Zhou, M.; Zhu, X. Application of DNA nanodevices for biosensing. *Analyst* **2020**, *145*, 3481–3489. [[CrossRef](#)]
12. Ayodele, O.; Adesina, A.; Pourianejad, S.; Averitt, J.; Ignatova, T. Recent Advances in Nanomaterial-Based Aptasensors in Medical Diagnosis and Therapy. *Nanomaterials* **2021**, *11*, 932. [[CrossRef](#)] [[PubMed](#)]
13. Ma, F.; Li, C.-C.; Zhang, C.-Y. Development of quantum dot-based biosensors: Principles and applications. *J. Mater. Chem. B* **2018**, *6*, 6173–6190. [[CrossRef](#)]
14. Kargozar, S.; Hoseini, S.J.; Milan, P.B.; Hooshmand, S.; Kim, H.; Mozafari, M. Quantum Dots: A Review from Concept to Clinic. *Biotechnol. J.* **2020**, *15*. [[CrossRef](#)] [[PubMed](#)]
15. Zhang, L.-J.; Xia, L.; Xie, H.-Y.; Zhang, Z.-L.; Pang, D.-W. Quantum Dot Based Biotracking and Biodetection. *Anal. Chem.* **2019**, *91*, 532–547. [[CrossRef](#)]
16. Wen, L.; Qiu, L.; Wu, Y.; Hu, X.; Zhang, X. Aptamer-Modified Semiconductor Quantum Dots for Biosensing Applications. *Sensors* **2017**, *17*, 1736. [[CrossRef](#)] [[PubMed](#)]
17. Foubert, A.; Beloglazova, N.V.; Rajkovic, A.; Sas, B.; Madder, A.; Goryacheva, I.Y.; De Saeger, S. Bioconjugation of quantum dots: Review & impact on future application. *TrAC Trends Anal. Chem.* **2016**, *83*, 31–48. [[CrossRef](#)]
18. Wagner, A.M.; Knipe, J.M.; Orive, G.; Peppas, N.A. Quantum dots in biomedical applications. *Acta Biomater.* **2019**, *94*, 44–63. [[CrossRef](#)]
19. Diaz-González, M.; De La Escosura-Muñiz, A.; Fernandez-Argüelles, M.T.; Alonso, F.J.G.; Costa-Fernandez, J.M. Quantum Dot Bioconjugates for Diagnostic Applications. *Top. Curr. Chem.* **2020**, *378*, 35. [[CrossRef](#)]
20. Taylor, A.I.; Holliger, P. Selecting Fully-Modified XNA Aptamers Using Synthetic Genetics. *Curr. Protoc. Chem. Biol.* **2018**, *10*, e44. [[CrossRef](#)]
21. Gatto, B.; Palumbo, M.; Sissi, C. Nucleic Acid Aptamers Based on the G-Quadruplex Structure: Therapeutic and Diagnostic Potential. *Curr. Med. Chem.* **2009**, *16*, 1248–1265. [[CrossRef](#)]
22. Kim, D.-M.; Go, M.-J.; Lee, J.; Na, D.; Yoo, S.-M. Recent Advances in Micro/Nanomaterial-Based Aptamer Selection Strategies. *Molecules* **2021**, *26*, 5187. [[CrossRef](#)]
23. Dunn, M.R.; Jimenez, R.M.; Chaput, J.C. Analysis of aptamer discovery and technology. *Nat. Rev. Chem.* **2017**, *1*, 0076. [[CrossRef](#)]
24. Cole, K.H.; Lupták, A. High-throughput methods in aptamer discovery and analysis. *Methods Enzymol.* **2019**, *621*, 329–346. [[CrossRef](#)] [[PubMed](#)]
25. Ni, S.; Zhuo, Z.; Pan, Y.; Yu, Y.; Li, F.; Liu, J.; Wang, L.; Wu, X.; Li, D.; Wan, Y.; et al. Recent Progress in Aptamer Discoveries and Modifications for Therapeutic Applications. *ACS Appl. Mater. Interfaces* **2021**, *13*, 9500–9519. [[CrossRef](#)] [[PubMed](#)]
26. Lyu, C.; Khan, I.M.; Wang, Z. Capture-SELEX for aptamer selection: A short review. *Talanta* **2021**, *229*, 122274. [[CrossRef](#)] [[PubMed](#)]
27. Stanciu, L.A.; Wei, Q.; Barui, A.K.; Mohammad, N. Recent Advances in Aptamer-Based Biosensors for Global Health Applications. *Annu. Rev. Biomed. Eng.* **2021**, *23*, 433–459. [[CrossRef](#)]
28. Tuerk, C.; Gold, L. Systematic Evolution of Ligands by Exponential Enrichment: RNA Ligands to Bacteriophage T4 DNA Polymerase. *Science* **1990**, *249*, 505–510. [[CrossRef](#)] [[PubMed](#)]
29. Ellington, A.D.; Szostak, J.W. In vitro selection of RNA molecules that bind specific ligands. *Nature* **1990**, *346*, 818–822. [[CrossRef](#)]
30. Bayat, P.; Nosrati, R.; Alibolandi, M.; Rafatpanah, H.; Abnous, K.; Khedri, M.; Ramezani, M. SELEX methods on the road to protein targeting with nucleic acid aptamers. *Biochimie* **2018**, *154*, 132–155. [[CrossRef](#)]
31. Matea, C.T.; Mocan, T.; Tabaran, F.; Pop, T.; Mosteanu, O.; Puia, C.; Iancu, C.; Mocan, L. Quantum dots in imaging, drug delivery and sensor applications. *Int. J. Nanomed.* **2017**, *12*, 5421–5431. [[CrossRef](#)] [[PubMed](#)]
32. Alivisatos, A.P. Semiconductor clusters, nanocrystals, and quantum dots. *Science* **1996**, *271*, 933–937. [[CrossRef](#)]
33. Michalet, X.; Pinaud, F.F.; Bentolila, L.A.; Tsay, J.M.; Doose, S.; Li, J.J.; Sundaresan, G.; Wu, A.M.; Gambhir, S.S.; Weiss, S. Quantum Dots for Live Cells, in Vivo Imaging, and Diagnostics. *Science* **2005**, *307*, 538–544. [[CrossRef](#)] [[PubMed](#)]
34. Ghosh, S.; Datta, D.; Chaudhry, S.; Dutta, M.; Stroschio, M.A. Rapid Detection of Tumor Necrosis Factor-Alpha Using Quantum Dot-Based Optical Aptasensor. *IEEE Trans. NanoBioscience* **2018**, *17*, 417–423. [[CrossRef](#)] [[PubMed](#)]
35. Ghosh, S.; Chen, Y.; Sebastian, J.; George, A.; Dutta, M.; Stroschio, M.A. A study on the response of FRET based DNA aptasensors in intracellular environment. *Sci. Rep.* **2020**, *10*, 13250. [[CrossRef](#)] [[PubMed](#)]

36. Ghosh, S.; Chen, Y.; George, A.; Dutta, M.; Stroschio, M.A. Fluorescence Resonant Energy Transfer-Based Quantum Dot Sensor for the Detection of Calcium Ions. *Front. Chem.* **2020**, *8*, 594. [[CrossRef](#)]
37. Medintz, I.L.; Mattoussi, H. Quantum dot-based resonance energy transfer and its growing application in biology. *Phys. Chem. Chem. Phys.* **2009**, *11*, 17–45. [[CrossRef](#)] [[PubMed](#)]
38. Jing, H.; Pálmai, M.; Saed, B.; George, A.; Snee, P.T.; Hu, Y.S. Cytosolic delivery of membrane-penetrating QDs into T cell lymphocytes: Implications in immunotherapy and drug delivery. *Nanoscale* **2021**, *13*, 5519–5529. [[CrossRef](#)]
39. Kovalenko, M.V.; Manna, L.; Cabot, A.; Hens, Z.; Talapin, D.V.; Kagan, C.R.; Klimov, V.I.; Rogach, A.L.; Reiss, P.; Milliron, D.J.; et al. Prospects of Nanoscience with Nanocrystals. *ACS Nano* **2015**, *9*, 1012–1057. [[CrossRef](#)]
40. Zhao, P.; Xu, Q.; Tao, J.; Jin, Z.; Pan, Y.; Yu, C.; Yu, Z. Near infrared quantum dots in biomedical applications: Current status and future perspective: Near infrared quantum dots in biomedical applications. *Wiley Interdiscip. Rev. Nanomed. Nanobiotechnol.* **2018**, *10*, e1483. [[CrossRef](#)]
41. De, C.K.; Routh, T.; Roy, D.; Mandal, S.; Mandal, P.K. Highly Photoluminescent InP Based Core Alloy Shell QDs from Air-Stable Precursors: Excitation Wavelength Dependent Photoluminescence Quantum Yield, Photoluminescence Decay Dynamics, and Single Particle Blinking Dynamics. *J. Phys. Chem. C* **2018**, *122*, 964–973. [[CrossRef](#)]
42. Ji, B.; Koley, S.; Slobodkin, I.; Remennik, S.; Banin, U. ZnSe/ZnS Core/Shell Quantum Dots with Superior Optical Properties through Thermodynamic Shell Growth. *Nano Lett.* **2020**, *20*, 2387–2395. [[CrossRef](#)] [[PubMed](#)]
43. Kim, T.; Kim, K.-H.; Kim, S.; Choi, S.-M.; Jang, H.; Seo, H.-K.; Lee, H.; Chung, D.-Y.; Jang, E. Efficient and stable blue quantum dot light-emitting diode. *Nature* **2020**, *586*, 385–389. [[CrossRef](#)] [[PubMed](#)]
44. Tan, J.; Guo, M.; Tan, L.; Geng, Y.; Huang, S.; Tang, Y.; Su, C.; Lin, C.C.; Liang, Y. Highly efficient fluorescent QDs sensor for specific detection of protein through double recognition of hybrid aptamer-molecular imprinted polymers. *Sens. Actuators B Chem.* **2018**, *274*, 627–635. [[CrossRef](#)]
45. Li, D.; Guo, J.; Zhao, L.; Zhang, G.; Yan, G. A label-free RTP sensor based on aptamer/quantum dot nanocomposites for cytochrome c detection. *RSC Adv.* **2019**, *9*, 31953–31959. [[CrossRef](#)]
46. Ren, J.; Liang, G.; Man, Y.; Li, A.; Jin, X.; Liu, Q.; Pan, L. Aptamer-based fluorometric determination of Salmonella Typhimurium using Fe<sub>3</sub>O<sub>4</sub> magnetic separation and CdTe quantum dots. *PLoS ONE* **2019**, *14*, e0218325. [[CrossRef](#)]
47. He, Z.-J.; Kang, T.-F.; Lu, L.-P.; Cheng, S.-Y. An electrochemiluminescence aptamer sensor for chloramphenicol based on GO-QDs nanocomposites and enzyme-linked aptamers. *J. Electroanal. Chem.* **2020**, *860*, 113870. [[CrossRef](#)]
48. Wang, J.; Jiang, X.; Han, H. Turn-on near-infrared electrochemiluminescence sensing of thrombin based on resonance energy transfer between CdTe/CdS coresmall/shellthick quantum dots and gold nanorods. *Biosens. Bioelectron.* **2016**, *82*, 26–31. [[CrossRef](#)]
49. Zhao, M.; Chen, A.-Y.; Huang, D.; Chai, Y.-Q.; Zhuo, Y.; Yuan, R. MoS<sub>2</sub> Quantum Dots as New Electrochemiluminescence Emitters for Ultrasensitive Bioanalysis of Lipopolysaccharide. *Anal. Chem.* **2017**, *89*, 8335–8342. [[CrossRef](#)]
50. Fan, Z.; Yao, B.; Ding, Y.; Xie, M.; Zhao, J.; Zhang, K.; Huang, W. Electrochemiluminescence aptasensor for Siglec-5 detection based on MoS<sub>2</sub>@Au nanocomposites emitter and exonuclease III-powered DNA walker. *Sens. Actuators B Chem.* **2021**, *334*, 129592. [[CrossRef](#)]
51. Wu, C.; Gan, N.; Ou, C.; Tang, H.; Zhou, Y.; Cao, J. A homogenous “signal-on” aptasensor for antibiotics based on a single stranded DNA binding protein-quantum dot aptamer probe coupling exonuclease-assisted target recycling for signal amplification. *RSC Adv.* **2017**, *7*, 8381–8387. [[CrossRef](#)]
52. Tang, J.; Huang, N.; Zhang, X.; Zhou, T.; Tan, Y.; Pi, J.; Pi, L.; Cheng, S.; Zheng, H.; Cheng, Y. Aptamer-conjugated PEGylated quantum dots targeting epidermal growth factor receptor variant III for fluorescence imaging of glioma. *Int. J. Nanomed.* **2017**, *12*, 3899–3911. [[CrossRef](#)] [[PubMed](#)]
53. Bruno, J.G.; Sivils, J.C. Further characterization and independent validation of a DNA aptamer-quantum dot-based magnetic sandwich assay for Campylobacter. *Folia Microbiol.* **2017**, *62*, 485–490. [[CrossRef](#)] [[PubMed](#)]
54. Li, L.; Li, Q.; Liao, Z.; Sun, Y.; Cheng, Q.; Song, Y.; Song, E.; Tan, W. Magnetism-Resolved Separation and Fluorescence Quantification for Near-Simultaneous Detection of Multiple Pathogens. *Anal. Chem.* **2018**, *90*, 9621–9628. [[CrossRef](#)]
55. Kurt, H.; Yüce, M.; Hussain, B.; Budak, H. Dual-excitation upconverting nanoparticle and quantum dot aptasensor for multiplexed food pathogen detection. *Biosens. Bioelectron.* **2016**, *81*, 280–286. [[CrossRef](#)] [[PubMed](#)]
56. Isildak, I.; Navaeipour, F.; Afsharan, H.; Kanberoglu, G.S.; Agir, I.; Ozer, T.; Annabi, N.; Totu, E.E.; Khalilzadeh, B. Electrochemiluminescence methods using CdS quantum dots in aptamer-based thrombin biosensors: A comparative study. *Microchim. Acta* **2019**, *187*, 25. [[CrossRef](#)]
57. Wang, Q.; Cheng, X.; Li, H.; Yu, F.; Wang, Q.; Yu, M.; Liu, D.; Xia, J. A novel DNA quantum dots/ aptamer-modified gold nanoparticles probe for detection of Salmonella typhimurium by fluorescent immunoassay. *Mater. Today Commun.* **2020**, *25*, 101428. [[CrossRef](#)]
58. Kitte, S.A.; Tafese, T.; Xu, C.; Saqib, M.; Li, H.; Jin, Y. Plasmon-enhanced quantum dots electrochemiluminescence aptasensor for selective and sensitive detection of cardiac troponin I. *Talanta* **2021**, *221*, 121674. [[CrossRef](#)]
59. Babamiri, B.; Salimi, A.; Hallaj, R. Switchable electrochemiluminescence aptasensor coupled with resonance energy transfer for selective attomolar detection of Hg<sup>2+</sup> via CdTe@CdS/dendrimer probe and Au nanoparticle quencher. *Biosens. Bioelectron.* **2018**, *102*, 328–335. [[CrossRef](#)]

60. Wang, Y.; Gan, N.; Li, T.; Cao, Y.; Hu, F.; Chen, Y. A novel aptamer–quantum dot fluorescence probe for specific detection of antibiotic residues in milk. *Anal. Methods* **2016**, *8*, 3006–3013. [[CrossRef](#)]
61. Tan, L.; Kang, C.; Xu, S.; Tang, Y. Selective room temperature phosphorescence sensing of target protein using Mn-doped ZnS QDs-embedded molecularly imprinted polymer. *Biosens. Bioelectron.* **2013**, *48*, 216–223. [[CrossRef](#)] [[PubMed](#)]
62. Aboulaich, A.; Geszke, M.; Balan, L.; Ghanbaja, J.; Medjahdi, G.; Schneider, R. Water-Based Route to Colloidal Mn-Doped ZnSe and Core/Shell ZnSe/ZnS Quantum Dots. *Inorg. Chem.* **2010**, *49*, 10940–10948. [[CrossRef](#)] [[PubMed](#)]
63. Zaidi, S.A. Molecular imprinting polymers and their composites: A promising material for diverse applications. *Biomater. Sci.* **2017**, *5*, 388–402. [[CrossRef](#)] [[PubMed](#)]
64. Jolly, P.; Tamboli, V.; Harniman, R.L.; Estrela, P.; Allender, C.J.; Bowen, J.L. Aptamer–MIP hybrid receptor for highly sensitive electrochemical detection of prostate specific antigen. *Biosens. Bioelectron.* **2016**, *75*, 188–195. [[CrossRef](#)] [[PubMed](#)]
65. Zhang, Z.; Liu, J. Molecularly Imprinted Polymers with DNA Aptamer Fragments as Macromonomers. *ACS Appl. Mater. Interfaces* **2016**, *8*, 6371–6378. [[CrossRef](#)] [[PubMed](#)]
66. Bai, W.; Spivak, D.A. A Double-Imprinted Diffraction-Grating Sensor Based on a Virus-Responsive Super-Aptamer Hydrogel Derived from an Impure Extract. *Angew. Chem. Int. Ed.* **2014**, *53*, 2095–2098. [[CrossRef](#)] [[PubMed](#)]
67. Ravindran, S.; Snee, P.T.; Ramachandran, A.; George, A. Acidic domain in dentin phosphophoryn facilitates cellular uptake: Implications in targeted protein delivery. *J. Biol. Chem.* **2013**, *288*, 16098–16109. [[CrossRef](#)] [[PubMed](#)]
68. Koshman, Y.E.; Waters, S.B.; Walker, L.A.; Los, T.; de Tombe, P.; Goldspink, P.H.; Russell, B. Delivery and visualization of proteins conjugated to quantum dots in cardiac myocytes. *J. Mol. Cell. Cardiol.* **2008**, *45*, 853–856. [[CrossRef](#)] [[PubMed](#)]
69. Xiong, E.; Zhang, X.; Liu, Y.; Zhou, J.; Yu, P.; Li, X.; Chen, J. Ultrasensitive Electrochemical Detection of Nucleic Acids Based on the Dual-Signaling Electrochemical Ratiometric Method and Exonuclease III-Assisted Target Recycling Amplification Strategy. *Anal. Chem.* **2015**, *87*, 7291–7296. [[CrossRef](#)]
70. Fu, X.; Tan, X.; Yuan, R.; Chen, S. A dual-potential electrochemiluminescence ratiometric sensor for sensitive detection of dopamine based on graphene-CdTe quantum dots and self-enhanced Ru(II) complex. *Biosens. Bioelectron.* **2017**, *90*, 61–68. [[CrossRef](#)]
71. Spring, S.; Goggins, S.; Frost, C. Ratiometric Electrochemistry: Improving the Robustness, Reproducibility and Reliability of Biosensors. *Molecules* **2021**, *26*, 2130. [[CrossRef](#)] [[PubMed](#)]
72. Lin, Y.; Wang, J.; Luo, F.; Guo, L.; Qiu, B.; Lin, Z. Highly reproducible ratiometric aptasensor based on the ratio of amplified electrochemiluminescence signal and stable internal reference electrochemical signal. *Electrochim. Acta* **2018**, *283*, 798–805. [[CrossRef](#)]
73. Zhang, Y.Y.; Zhou, H.; Wu, P.; Zhang, H.R.; Xu, J.J.; Chen, H.Y. In situ activation of CdS electrochemiluminescence film and its application in H<sub>2</sub>S detection. *Anal. Chem.* **2014**, *86*, 8657–8664. [[CrossRef](#)] [[PubMed](#)]
74. Cai, F.; Zhu, Q.; Zhao, K.; Deng, A.; Li, J. Multiple Signal Amplified Electrochemiluminescent Immunoassay for Hg<sup>2+</sup> Using Graphene-Coupled Quantum Dots and Gold Nanoparticles-Labeled Horseradish Peroxidase. *Environ. Sci. Technol.* **2015**, *49*, 5013–5020. [[CrossRef](#)] [[PubMed](#)]
75. Delices, A.; Moodelly, D.; Hurot, C.; Hou, Y.; Ling, W.L.; Saint-Pierre, C.; Gasparutto, D.; Nogues, G.; Reiss, P.; Kheng, K. Aqueous synthesis of DNA-functionalized near-infrared AgInS<sub>2</sub>/ZnS core/shell quantum dots. *ACS Appl. Mater. Interfaces* **2020**, *12*, 44026–44038. [[CrossRef](#)] [[PubMed](#)]
76. Xu, L.; Kuang, H.; Wang, L.; Xu, C. Gold nanorod ensembles as artificial molecules for applications in sensors. *J. Mater. Chem.* **2011**, *21*, 16759–16782. [[CrossRef](#)]
77. Wang, J.; Han, H.-Y. Near-infrared electrogenerated chemiluminescence from quantum dots. *Rev. Anal. Chem.* **2013**, *32*, 43. [[CrossRef](#)]
78. Stobiecka, M. Novel plasmonic field-enhanced nanoassay for trace detection of proteins. *Biosens. Bioelectron.* **2014**, *55*, 379–385. [[CrossRef](#)]
79. Stobiecka, M.; Chalupa, A. Modulation of Plasmon-Enhanced Resonance Energy Transfer to Gold Nanoparticles by Protein Survivin Channeled-Shell Gating. *J. Phys. Chem. B* **2015**, *119*, 13227–13235. [[CrossRef](#)]
80. Kim, D.M.; Yoo, S.M. DNA-modifying enzyme reaction-based biosensors for disease diagnostics: Recent biotechnological advances and future perspectives. *Crit. Rev. Biotechnol.* **2020**, *40*, 787–803. [[CrossRef](#)]
81. Gopalakrishnan, D.; Damien, D.; Shaijumon, M.M. MoS<sub>2</sub> Quantum Dot-Interspersed Exfoliated MoS<sub>2</sub> Nanosheets. *ACS Nano* **2014**, *8*, 5297–5303. [[CrossRef](#)] [[PubMed](#)]
82. Wang, Z.; Tang, M. The cytotoxicity of core-shell or non-shell structure quantum dots and reflection on environmental friendly: A review. *Environ. Res.* **2020**, *194*, 110593. [[CrossRef](#)] [[PubMed](#)]
83. Ye, J.; Zhu, L.; Yan, M.; Zhu, Q.; Lu, Q.; Huang, J.; Cui, H.; Yang, X. Dual-Wavelength Ratiometric Electrochemiluminescence Immunosensor for Cardiac Troponin I Detection. *Anal. Chem.* **2019**, *91*, 1524–1531. [[CrossRef](#)]
84. Du, Y.; Zhong, Y.; Dong, J.; Qian, C.; Sun, S.; Gao, L.; Yang, D. The effect of PEG functionalization on the in vivo behavior and toxicity of CdTe quantum dots. *RSC Adv.* **2019**, *9*, 12218–12225. [[CrossRef](#)]
85. Zhang, L.; Dou, X.; Zhang, C.; Ying, G.; Liu, C.; Luo, J.; Li, Q.; Li, P.; Wang, Y.; Yang, M. Facile preparation of stable PEG-functionalized quantum dots with glycine-enhanced photoluminescence and their application for screening of aflatoxin B1 in herbs. *Sens. Actuators B Chem.* **2018**, *261*, 188–195. [[CrossRef](#)]

86. Lemon, C.M.; Karnas, E.; Han, X.; Bruns, O.T.; Kempa, T.J.; Fukumura, D.; Bawendi, M.G.; Jain, R.K.; Duda, D.G.; Nocera, D.G. Micelle-Encapsulated Quantum Dot-Porphyrin Assemblies as in Vivo Two-Photon Oxygen Sensors. *J. Am. Chem. Soc.* **2015**, *137*, 9832–9842. [[CrossRef](#)] [[PubMed](#)]
87. Chinnathambi, S.; Abu, N.; Hanagata, N. Biocompatible CdSe/ZnS quantum dot micelles for long-term cell imaging without alteration to the native structure of the blood plasma protein human serum albumin. *RSC Adv.* **2017**, *7*, 2392–2402. [[CrossRef](#)]
88. Wang, Y.; Wang, Y.; Chen, G.; Li, Y.; Xu, W.; Gong, S. Quantum-Dot-Based Theranostic Micelles Conjugated with an Anti-EGFR Nanobody for Triple-Negative Breast Cancer Therapy. *ACS Appl. Mater. Interfaces* **2017**, *9*, 30297–30305. [[CrossRef](#)]
89. Kim, Y.H.; Lee, H.; Kang, S.-M.; Bae, B.-S. Two-Step-Enhanced Stability of Quantum Dots via Silica and Siloxane Encapsulation for the Long-Term Operation of Light-Emitting Diodes. *ACS Appl. Mater. Interfaces* **2019**, *11*, 22801–22808. [[CrossRef](#)]
90. Kim, Y.H.; Koh, S.; Lee, H.; Kang, S.-M.; Lee, D.C.; Bae, B.-S. Photo-Patternable Quantum Dots/Siloxane Composite with Long-Term Stability for Quantum Dot Color Filters. *ACS Appl. Mater. Interfaces* **2020**, *12*, 3961–3968. [[CrossRef](#)]
91. Choi, Y.; Lee, S.Y. Biosynthesis of inorganic nanomaterials using microbial cells and bacteriophages. *Nat. Rev. Chem.* **2020**, *4*, 638–656. [[CrossRef](#)]
92. Mi, C.; Wang, Y.; Zhang, J.; Huang, H.; Xu, L.; Wang, S.; Fang, X.; Fang, J.; Mao, C.; Xu, S. Biosynthesis and characterization of CdS quantum dots in genetically engineered *Escherichia coli*. *J. Biotechnol.* **2011**, *153*, 125–132. [[CrossRef](#)] [[PubMed](#)]
93. Ulloa, G.; Collao, B.; Araneda, M.; Escobar, B.; Álvarez, S.; Bravo, D.; Pérez-Donoso, J. Use of acidophilic bacteria of the genus *Acidithiobacillus* to biosynthesize CdS fluorescent nanoparticles (quantum dots) with high tolerance to acidic pH. *Enzym. Microb. Technol.* **2016**, *95*, 217–224. [[CrossRef](#)]
94. Carrasco, V.; Amarelle, V.; Lagos-Moraga, S.; Quezada, C.P.; Espinoza-González, R.; Faccio, R.; Fabiano, E.; Pérez-Donoso, J.M. Production of cadmium sulfide quantum dots by the lithobiontic Antarctic strain *Pedobacter* sp. UYP1 and their application as photosensitizer in solar cells. *Microb. Cell Factories* **2021**, *20*, 41. [[CrossRef](#)] [[PubMed](#)]
95. Moon, J.-W.; Ivanov, I.N.; Duty, C.E.; Love, L.J.; Rondinone, A.J.; Wang, W.; Li, Y.-L.; Madden, A.S.; Mosher, J.J.; Hu, M.Z.; et al. Scalable economic extracellular synthesis of CdS nanostructured particles by a non-pathogenic thermophile. *J. Ind. Microbiol. Biotechnol.* **2013**, *40*, 1263–1271. [[CrossRef](#)] [[PubMed](#)]
96. Órdenes-Aenishanslins, N.; Anziani-Ostuni, G.; Monrás, J.P.; Tello, A.; Bravo, D.; Toro-Ascuy, D.; Rifo, R.S.; Prasad, P.N.; Pérez-Donoso, J.M. Bacterial Synthesis of Ternary CdS/Ag Quantum Dots through Cation Exchange: Tuning the Composition and Properties of Biological Nanoparticles for Bioimaging and Photovoltaic Applications. *Microorganisms* **2020**, *8*, 631. [[CrossRef](#)] [[PubMed](#)]
97. Monrás, J.P.; Diaz, V.; Bravo, D.; Montes, R.A.; Chasteen, T.G.; Osorio-Roman, I.O.; Vásquez, C.C.; Pérez-Donoso, J.M. Enhanced Glutathione Content Allows the In Vivo Synthesis of Fluorescent CdTe Nanoparticles by *Escherichia coli*. *PLoS ONE* **2012**, *7*, e48657. [[CrossRef](#)]
98. Moon, J.W.; Ivanov, I.N.; Joshi, P.C.; Armstrong, B.L.; Wang, W.; Jung, H.; Rondinone, A.J.; Jellison, G.E.; Meyer, H.M., Jr.; Jang, G.G., 3rd; et al. Scalable production of microbially mediated zinc sulfide nanoparticles and application to functional thin films. *Acta Biomater.* **2014**, *10*, 4474–4483. [[CrossRef](#)] [[PubMed](#)]
99. Moon, J.-W.; Phelps, T.J.; Fitzgerald, C.L., Jr.; Lind, R.F.; Elkins, J.G.; Jang, G.G.; Joshi, P.C.; Kidder, M.; Armstrong, B.L.; Watkins, T.R.; et al. Manufacturing demonstration of microbially mediated zinc sulfide nanoparticles in pilot-plant scale reactors. *Appl. Microbiol. Biotechnol.* **2016**, *100*, 7921–7931. [[CrossRef](#)] [[PubMed](#)]
100. Dameron, C.T.; Reese, R.N.; Mehra, R.K.; Kortan, A.R.; Carroll, P.J.; Steigerwald, M.L.; Brus, L.E.; Winge, D.R. Biosynthesis of cadmium sulphide quantum semiconductor crystallites. *Nature* **1989**, *338*, 596–597. [[CrossRef](#)]
101. Al-Shalabi, Z.; Doran, P.M. Biosynthesis of fluorescent CdS nanocrystals with semiconductor properties: Comparison of microbial and plant production systems. *J. Biotechnol.* **2016**, *223*, 13–23. [[CrossRef](#)]
102. Syed, A.; Ahmad, A. Extracellular biosynthesis of CdTe quantum dots by the fungus *Fusarium oxysporum* and their anti-bacterial activity. *Spectrochim. Acta A Mol. Biomol. Spectrosc.* **2013**, *106*, 41–47. [[CrossRef](#)] [[PubMed](#)]
103. Bao, H.; Hao, N.; Yang, Y.; Zhao, D. Biosynthesis of biocompatible cadmium telluride quantum dots using yeast cells. *Nano Res.* **2010**, *3*, 481–489. [[CrossRef](#)]
104. Mala, J.G.S.; Rose, C. Facile production of ZnS quantum dot nanoparticles by *Saccharomyces cerevisiae* MTCC 2918. *J. Biotechnol.* **2014**, *170*, 73–78. [[CrossRef](#)] [[PubMed](#)]
105. Jacob, J.M.; Rajan, R.; Kurup, G.G. Biologically synthesized ZnS quantum dots as fluorescent probes for lead (II) sensing. *Luminescence* **2020**, *35*, 1328–1337. [[CrossRef](#)] [[PubMed](#)]
106. Hou, L.; Gao, F.; Li, N. T4 Virus-Based Toolkit for the Direct Synthesis and 3D Organization of Metal Quantum Particles. *Chemistry* **2010**, *16*, 14397–14403. [[CrossRef](#)]
107. Mao, C.; Flynn, C.E.; Hayhurst, A.; Sweeney, R.; Qi, J.; Georgiou, G.; Iverson, B.; Belcher, A.M. Viral assembly of oriented quantum dot nanowires. *Proc. Natl. Acad. Sci. USA* **2003**, *100*, 6946–6951. [[CrossRef](#)]
108. Huang, F.; Dang, Z.; Guo, C.-L.; Lu, G.-N.; Gu, R.R.; Liu, H.-J.; Zhang, H. Biosorption of Cd(II) by live and dead cells of *Bacillus cereus* RC-1 isolated from cadmium-contaminated soil. *Colloids Surf. B Biointerfaces* **2013**, *107*, 11–18. [[CrossRef](#)]
109. He, X.; Ma, N. An overview of recent advances in quantum dots for biomedical applications. *Colloids Surf. B Biointerfaces* **2014**, *124*, 118–131. [[CrossRef](#)]

- 
110. Wang, F.-T.; Wang, L.-N.; Xu, J.; Huang, K.-J.; Wu, X. Synthesis and modification of carbon dots for advanced biosensing application. *Analyst* **2021**, *146*, 4418–4435. [[CrossRef](#)]
  111. Sivasankarapillai, V.S.; Jose, J.; Shanavas, M.S.; Marathakam, A.; Uddin, S.; Mathew, B. Silicon Quantum Dots: Promising Theranostic Probes for the Future. *Curr. Drug Targets* **2019**, *20*, 1255–1263. [[CrossRef](#)] [[PubMed](#)]